The application of a multi-wavelength Aethalometer to estimate iron dust and black carbon concentrations in the marine boundary layer of Cape Verde

P. Fialho[1*], M. Cerqueira[2], C. Pio[2], J. Cardoso[2,3], T. Nunes[2], D. Custódio[2], C. Alves[2], S. M. Almeida[4], M.Almeida-Silva[4], M. Reis[4], F. Rocha[5]

[1]*University of Azores, Rua Capitão João de Ávila, PT9700-042 Angra do Heroísmo, Portugal*

[2] *Department of Environment and Planning & CESAM, University of Aveiro, 3810-193 Aveiro, Portugal*

[3] *University of Cape Verde, Campus do Palmarejo, CP-279, Praia, Cape Verde*

[4] *Centro de Ciências e Tecnologias Nucleares, Instituto Superior Técnico, Universidade de Lisboa, 2695-066 Bobadela LRS, Portugal*

[5]*Department of Geosciences, GeoBioTec – GeoBioSciences, Geotechnologies and Geoengineering Research Center, University of Aveiro, 3810-193 Aveiro, Portugal*

*Corresponding author: Telephone: +351 295 402 560; Fax: +351 295 402 205; Email address: fialho.paulo@gmail.com

Abstract

The two-component model (Fialho et al., 2006) was used to decouple the contributions of black carbon (BC) and iron oxides, present in dust, to the aerosol attenuation coefficient, measured with a multi-wavelength Aethalometer. The model results were compared with the elemental carbon (EC) and iron concentrations determined in the laboratory from the analysis of aerosol particles collected with conventional samplers. The comparison was based on one year of data obtained at Praia, Santiago Island, Cape Verde, after side by side operation of the aerosol monitoring instruments. The linear regression equation that best describes the relationship between BC concentrations, derived from the Aethalometer, and EC concentrations, derived from a PM_{10} high-volume sampler after filter analysis with a thermal optical method, presents a slope of 1.01±0.05 and a correlation coefficient (*r*) of 0.90, showing that the model worked as intended to describe BC concentrations without interferences from iron dust. On the other hand, the linear regression equation that best describes the relationship between the iron concentrations derived from the Aethalometer and elemental iron concentrations, derived from a PM_{10} low-volume sampler after filter analysis by k_0 - Instrumental Neutron Activation Analysis, presents a slope of 0.495±0.014 and a correlation coefficient (*r*) of 0.96. These results show that the two-component model underestimated the iron concentrations in dust aerosol, which was explained by differences in the size range of particles sampled with the Aethalometer and the PM_{10} low-volume sampler together with differences in the size distribution of iron oxides.

Keywords: iron dust; black carbon; Aethalometer; two-component model; Cape Verde

1. Introduction

The African continent is an important source of mineral dust and biomass burning particles to the global atmosphere (Prospero et al., 2002, Langmann et al., 2009). These particles are known to affect the Earth's radiative budget (Satheesh and Krishna Moorthy, 2005; Langmann et al., 2009), to influence cloud formation and precipitation (DeMott et al., 2003; Lin et al., 2006; Petters et al., 2009) and to play an important role in biogeochemical cycles (Crutzen and Andreae, 1990; Mahowald et al., 2005). The radiative effects of these particles are strongly related with their chemical composition (Haywood and Boucher, 2000; Satheesh and Krishna Moorthy, 2005). Iron oxides and black carbon (BC) are major light absorbing constituents, at visible wavelengths, of dust and combustion particles, respectively, (Bohren and Huffman, 1998; Bond and Bergstrom, 2006; Linke et al., 2006), thus contributing to the aerosol attenuation coefficient and affecting the radiative transfer within the atmosphere.

BC in atmospheric sciences is operationally defined as the light absorbing fraction of carbonaceous aerosols and is usually determined through the measurement of light attenuation by particles collected on a filter. However, optical techniques can provide erroneous estimates of BC, due to the presence of mineral dust. Previous studies dealing with this effect have shown that the contribution of dust aerosol to optical absorption can be as great as 30% (Jennings et al., 1996; Pinnick et al., 1993; Coen et al., 2003; Bodhaine, 1995; Hansen et al., 1993).

Previously, Fialho *et al.* (2005) proposed a two-component model to decouple the contribution of BC and dust from the aerosol attenuation coefficient measured with the Aethalometer.

$$\sigma_{ATN-aerosol}(\lambda,t) = \sigma_{BC}(\lambda,t) + \sigma_{dust}(\lambda,t) \quad (1.1)$$

where $\sigma_{ATN\text{-}aerosol}(\lambda,t)$ is the Aethalometer aerosol attenuation coefficient, $\sigma_{BC}(\lambda,t)$ and $\sigma_{dust}(\lambda,t)$ are, respectively, the BC and dust Aethalometer attenuation coefficients.

The two-component model was further developed by Fialho *et al.* (2006), after experimental determination of the calibration coefficient for elemental iron (used as an indicator of light attenuation due to the presence of iron oxide in dust aerosol and considering that dust color is the result of the overwhelming abundance of hematite, Fe_2O_3 (red), and goethite, FeO(OH) (yellowish brown), in soils with low concentrations of organic matter, such as deserts (Torrent et al., 1983).

$$\sigma_{ATN-aerosol}(\lambda,t) = 14.625 \times \lambda^{-1} \times C_{BC}(t) + 0.234 \times \lambda^{-4} \times C_{Fe}(t) \quad (1.2)$$

Where, $C_{BC}(t)$ and $C_{Fe}(t)$ are, respectively, the concentrations of BC and elemental iron, and the numbers are the calibration constants for BC (14.625 $\mu m.m^2g^{-1}$, used by the Aethalometer (Hansen, 2003)) and elemental iron (0.234 $\mu m^4m^2g^{-1}$, estimated in Fialho *et al.* (2006)).

The purpose of this work is to test the two-component model described above by comparing the BC and iron concentration results obtained with a multi-wavelength Aethalometer with the elemental carbon (EC) and elemental iron concentrations determined in the laboratory from the analysis of aerosol particles collected with conventional high and low volume filter samplers. Although the operational definition of BC is different from that of EC, which is the aerosol carbon fraction that is oxidized in combustion analysis above a certain temperature threshold (Andreae & Gelencsér, 2006), both terms are often used interchangeably and are commonly well correlated (Allen et al., 1999; Park et al., 2002). Therefore EC is assumed to be an appropriate parameter to evaluate the Aethalometer performance.

This comparison study is based on one year of data obtained at Santiago Island (Cape Verde), within the framework of CV-Dust research project, after side by side operation of the aerosol

monitoring and sampling instruments. Aerosol in the Cape Verde area has very often been observed to be a mixture of dust particles transported from the Sahara desert and carbon particles resulting from biomass burning practices in the region south of the Sahel (Lieke et al., 2011; Tesche et al., 2011) and from local traffic emissions (Gonçalves et al., 2014), and therefore the islands are ideally located to explore the two-component model capabilities.

The present work assumes that the enhancement of the aerosol attenuation coefficient with the wavelength was solely the result of iron in aerosol particles. Atmospheric "brown" carbon, which is also known to enhance the Aethalometer attenuation signal (Andreae and Gelencsér, 2006), was neglected considering the very low concentrations of levoglucosan (an acknowledged biomass burning tracer) reported by Gonçalves et al. (2014) during the CV-Dust field experiment (2 to 10 ng/m^3).

2. Experimental setup and working equations

2.1 Sampling site

Aerosol sampling was performed from January 12 through December 30, 2011, at the former airport of Praia, in the south-eastern edge of Santiago Island, Cape Verde (14º 55' N; 23º 29 ´W; 98 m a.s.l.). The site is located to the east of the urban settlement of Praia and prevalent winds are north-easterlies (trade winds) transporting particles from mainland Africa. However, local anthropogenic influences on aerosol composition cannot be precluded.

2.2 Aerosol attenuation coefficient measurements

A seven wavelength Aethalometer (Magee Scientific, model AE31, λ = 370, 470, 520, 590, 660, 880 and 950 nm) equipped with a "high sensitivity" circular spot size chamber was used to measure the aerosol attenuation coefficient. Ambient air was sampled at a flow rate of 4.0 dm^3/min, measured with the internal Aethalometer mass flowmeter (Sierra Model 824), through a whole air inlet without any specific cut-off size. The inlet setup consisted of one tube (length: 1.5 m; internal diameter: 6.0 mm) extending horizontally from an open window, with the opening slightly falling down. The inlet efficiency was estimated with the aerosol calculator program developed by Baron (2001), assuming spherical particles with densities between 1 and 4 g/cm^3 and diameters between 1 µm and 10 µm, and isokinetic sampling conditions (Table 1).

Table 1 – Inlet efficiency for an isoaxial horizontal tube and isokinetic sampling conditions (Baron, 2001).

Particle diameter (μm)	Particle density (g/cm^3)		
	1.0	**2.0**	**4.0**
1.0	0.97	0.96	0.93
2.5	0.91	0.85	0.76
5.0	0.77	0.64	0.47
10	0.48	0.29	0.12

Particulate matter accumulated in a quartz fibre filter tape (Q250F from Pallflex©) and the instrument was setup to automatically advance the tape whenever the ATN (370 nm) sign was higher than 50% to avoid significant overloading of the filter with aerosol. The impact of the loading effect correction will be discussed below, in section 3.2. From January 12 to April 7, at 10 a.m., the sampling period was set to 5 minutes; after that, until the end of the experiment (December 30, at 12 a.m.) it was set to 2 minutes, in order to decrease the time gaps between the automatic Aethalometer filter changes. The Aethalometer was setup to report the mass in μg/m^3 of equivalent BC and the instrument detection limit was 0.1 μg/m^3. The Aethalometer was removed from the sampling site between December 13 and December 23, to be used in an intercomparison experiment. Therefore, measurements are not available for that period.

2.3 EC and iron-containing aerosols measurements

Aerosol particles were collected simultaneously with a high-volume sampler (Tisch) and a low-volume sampler (TCR Tecora) both equipped with PM_{10} size selective inlets. Sampling periods were irregular and dependent on the filter loading. During Saharan dust episodes dust accumulation was faster and sampling periods were shorter than those of the non-dust episodes. The average sampling period was of 2 days and 16 hours, with a sample range of 7 hours to 6 days and 22 hours, depending on the mass of particles accumulated in the filters. Quartz fibre filters and Nuclepore polycarbonate filters were used with the high-volume and the low-volume sampler, respectively. Elemental carbon was analysed in the quartz filters using a home-made thermal-optical system, based on the thermal desorption/oxidation of particulate carbon to CO_2, that is subsequently measured by non-dispersive infrared spectrophotometry (Castro et al., 1999; Pio et al, 2011). This method was tested with the NIST (National Institute of Standards and Technology) 8785 filter standard and in an intercomparison experiment with real aerosol samples (Schmid et al., 2001), delivering results between those obtained by the NIOSH (National Institute for Occupational Safety and Health) 5040 and the IMPROVE (Interagency Monitoring of Protected Visual Environments) protocols, but closer to the latter. The method detection limit was 30 ng/m^3. Iron was measured in

the polycarbonate filters by k_0 - Instrumental Neutron Activation Analysis (k_0-INAA) as described by Almeida et al. (2008) and Almeida et al. (2013). Results obtained with k_0-INAA were compared with iron measurements performed in the same filters by particle induced X-ray emission (PIXE) and revealed a good correlation between the two methods (regression coefficient of 0.97, with a slope of 0.976 and an intercept of 0.18 μg/m^3; Almeida-Silva *et al.*, 2014). The k_0-INAA detection limit was found to be 55 ng/m^3.

2.4. Aethalometer working equations

The reported Aethalometer particle aerosol concentrations, $C_{AE}(\lambda, t)$, were averaged into the 10 minute interval, by calculating the moving averages of the 5 and 2 minute sampled data.

Application of Eq.(1.2), to these data, needs the calculation of the particle aerosol attenuation coefficient, $\sigma_{ATN\text{-}aerosol}(\lambda, t)$, which is done by using equation (2),

$$\sigma_{ATN-aerosol}\left(\lambda,t;Mm^{-1}\right)=14.625\left(\mu m\, m^2 g^{-1}\right)\times\lambda(\mu m)^{-1}\times C_{AE}\left(\lambda,t;\mu g.m^{-3}\right) \quad (2)$$

Estimation of, $C_{BC}(t)$ and $C_{Fe}(t)$, was done by considering only the particle aerosol attenuation coefficient, $\sigma_{ATN\text{-}aerosol}(\lambda, t)$, at the visible wavelengths (0.47, 0.52, 0.59 and 0.66 μm - as suggested by Fialho *et al.* (2006)), and by linear fitting Eq.(1.2) rearranged in the forms,

$$\underbrace{\sigma_{ATN-aerosol}(\lambda,t)\times\lambda}_{y_{3.1}(\lambda,t)}=\underbrace{14.625\times C_{BC}(t)}_{\text{intercept}_{3.1}}+\underbrace{0.234\times C_{Fe}(t)}_{slope_{3.1}}\times\underbrace{\lambda^{-3}}_{x_{3.1}(\lambda)} \quad (3.1)$$

$$\underbrace{\sigma_{ATN-aerosol}(\lambda,t)\times\lambda^4}_{y_{3.2}(\lambda,t)}=\underbrace{14.625\times C_{BC}(t)}_{\text{slope}_{3.2}}\times\underbrace{\lambda^3}_{x_{3.2}(\lambda)}+\underbrace{0.234\times C_{Fe}(t)}_{\text{intercept}_{3.2}} \quad (3.2)$$

From each fit the correlation coefficients, $r_{3.1}$ and $r_{3.2}$, were calculated and the following considerations were made:

- if $\text{slope}_{3.1}$ was positive and $r_{3.1}$ greater than 0.7, or, $\text{slope}_{3.2}$ was positive and $r_{3.2}$ greater than 0.7, the two-component model given by Eq.(1) was adopted and, the best solution was decided in favour of the one with the highest correlation coefficient, $r_{3.1}$ or $r_{3.2}$.
- in the other situations, the average value of $C_{AE}(\lambda, t)$, calculated from considering only the visible wavelengths, was taken as the best estimation of $C_{BC}(t)$, and $C_{Fe}(t)$ was assumed to be zero.

The threshold of $r > 0.7$, is the limit at which the two-component model can explain at least 50% of the experimental attenuation signal as being a contribution from the presence of at least one of

the two types of aerosol components (BC and/or iron oxides). The selection of Eq.(3.1) or Eq.(3.2) is most significant when at least one of the aerosol constituents has concentrations near the limit of detection of the method. Taking this under consideration, equation (3), which multiplies that aerosol constituent concentration by the slope, should be disregarded in favour of the other.

When the Aethalometer aerosol attenuation coefficient is near the limit of detection, it is not possible to get a good correlation coefficient for either one of the equations (3.1 or 3.2). The value is then averaged and associated to BC aerosol concentration and the iron oxide contribution is assumed to be zero.

To compare the Aethalometer $C_{BC}(t)$ and $C_{Fe}(t)$ with the values obtained from the high-volume (HV) and low-volume (LV) filter analysis, the Aethalometer data were averaged for the same time period of those samplers and the corresponding overlap coverage (AE_HLV), was calculated by the equation,

$$\mathrm{AE\_HLV} = \frac{\sum_{\text{start HLV sampling period}}^{\text{end HLV sampling period}} \textit{Aethalometer sampling period}}{\textit{HLV samping period}} \times 100\% \quad (4)$$

where HLV stands for high and low volume. For the estimation of the correlation models only the periods with more than 70% of overlap coverage were used.

In reality, the interval is in the range of 70% to 130%; values of AE_HLV larger than 100% result from the fact that the HV and LV samplers have been operating with interruptions and in some cases the effective sampling period for these instruments was shorter than the registered sampling period of the Aethalometer filter tape (a consequence of power failures and restart of both systems without synchronization); whenever we mention more than 70% along this paper, we are referring to the]70%,130%[interval.

3. Results and discussion

3.1 Model performance for predicting BC and iron concentrations in aerosols

Figure 1 shows time series of Aethalometer particle aerosol concentrations, $C_{AE}(\lambda, t)$ and respective angstrom exponents at the sampling site of Praia, during the month of February. Angstrom exponents higher than 2.5 were observed during two periods in early and late February. These maxima coincided with peak values of atmospheric dust (Pio et al., 2014) and were related with air mass transport from Western Sahara (Figure 2). Dust episodes like these are common in the Cape Verde islands and illustrate the importance of using a decoupling model to separate the contributions of different species to the aerosol attenuation coefficient.

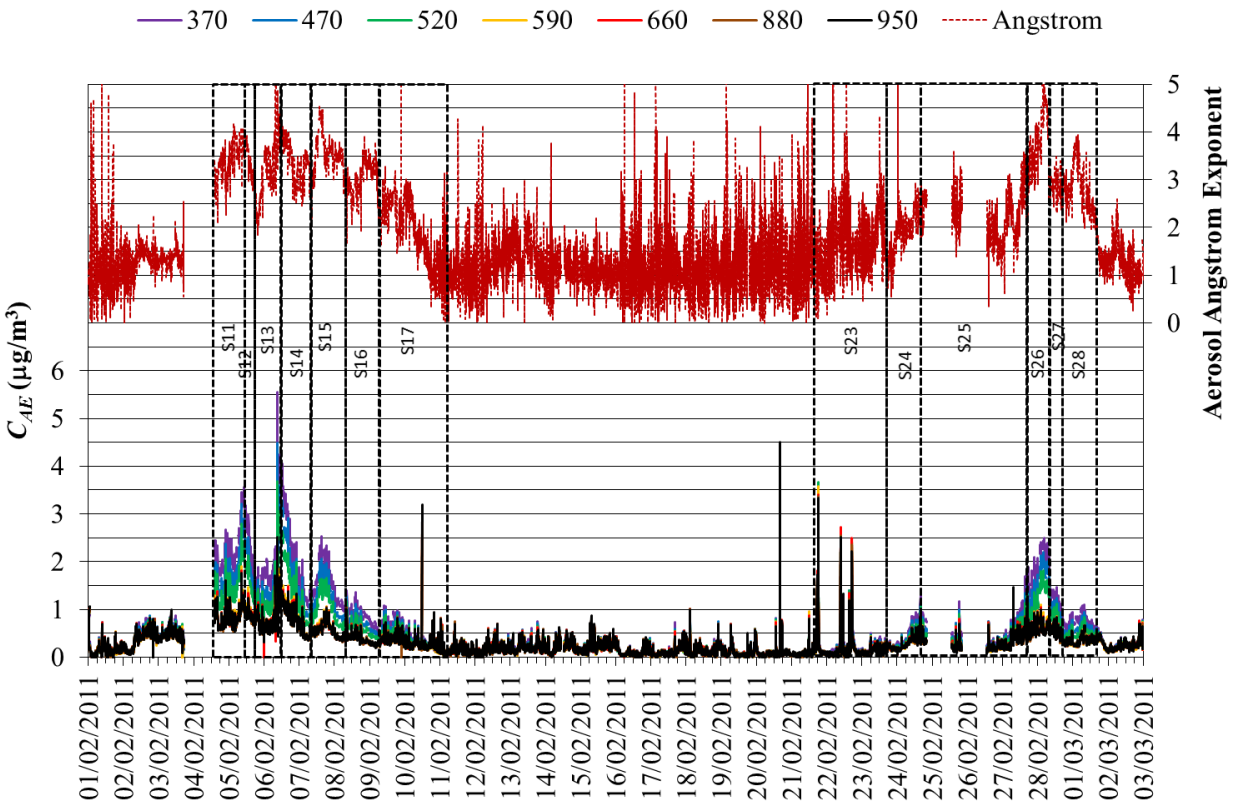

Figure 1 – Time series of 10 minute Aethalometer particle aerosol concentrations, $C_{AE}(\lambda, t)$ and respective angstrom exponents obtained from the four visible wavelengths, during February 2011. The coloured solid lines in the legend identify the seven wavelength values and the red dotted line is the angstrom exponent. The black dotted boxes define the HV and LV sampling periods (S11 to S17 and S23 to S28).

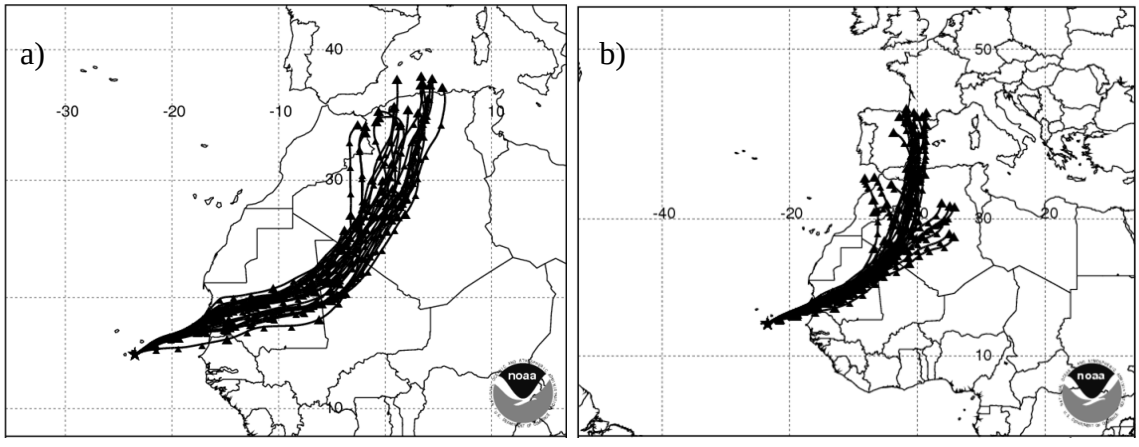

Figure 2 – Four-day back trajectories, arriving every hour at the sampling site, from February 5 to February 10 (a) and from February 27 to March 3 (b), calculated with the HYSPLIT model (Draxler and Rolph, 2013). The black triangles denote 6 h intervals.

Figure 3-a) shows the black carbon concentrations obtained from the Aethalometer measurements after applying the two-component model presented by Eq.3 and averaging the data for the HV filter sampling interval, together with the elemental carbon determined in the laboratory from the analysis of HV samples. Figure 3-b) shows the elemental iron concentrations obtained from the Aethalometer measurements after applying the two-component model presented by Eq.3 and averaging the data for the LV filter sampling interval together with the elemental iron determined in the laboratory from the analysis of the LV samples.

The time series of Figures 3a) and 3b) present all the data regardless of the gaps between the sampling periods of the two instruments. The criterion of the 70% overlap seems to work well for the majority of the data, although, for a few points, the deviations between the concentration values obtained with both techniques could be significant. Those differences can be easily explained by the fact that the ambient aerosol concentration was changing during the sampling period and simultaneously one of the sampling instruments was not working.

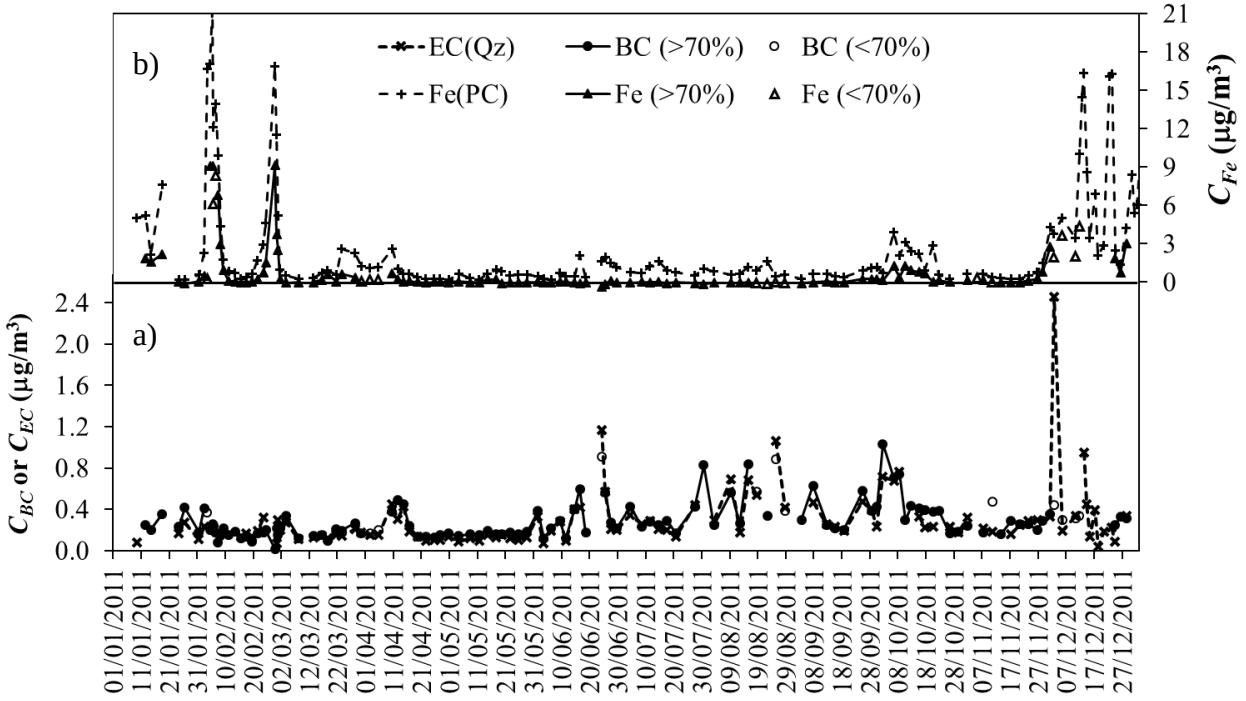

Figure 3 – Time series of black carbon (C_{BC}), elemental carbon (C_{EC}) and elemental iron (C_{Fe}) concentrations determined during 2011 at the outskirts of Praia, Santiago Island, in Cape Verde. The concentration values are averages reported for the HLV sampling periods. a) Black dots connected by a black solid line represent black carbon concentrations, estimated with the Aethalometer, for periods where the overlapping with the HLV sampling was greater than 70%. Empty circles represent black carbon concentrations, estimated with the Aethalometer, for periods where the overlapping with

the HLV sampling was less than 70%. Black crosses connected by a dotted black line are elemental carbon concentrations estimated from the laboratory analysis of the HV quartz filters (Qz). b) Black triangles connected by a black solid line represent elemental iron concentrations, estimated with the Aethalometer, for periods where the overlapping with the HLV sampling was greater than 70%. Empty triangles represent elemental iron concentrations, estimated with the Aethalometer, for periods where the overlapping with the HLV sampling was less than 70%. Black crosses connected by a dotted black line are elemental iron concentrations estimated from the laboratory analysis of the LV polycarbonate (PC) filters.

Analysis of Figure 3-a) shows that, C_{BC} and C_{EC}, present a similar behaviour. A linear regression was performed to quantify this correlation (Figure 4), and only the pairs of points for which the Aethalometer information overlapped the HV samples by at least 70% (84 - black dots) were used for this purpose. Eq.(5) is the model that results from this correlation analysis with a standard error of 0.08 μg/m^3 and a correlation coefficient, *r*, of 0.90.

$$C_{BC}\left(\mu g / m^3\right) = \left(0.033 \pm 0.016\right) + \left(1.01 \pm 0.05\right) \times C_{EC}\left(\mu g / m^3\right) \quad (5)$$

The slope of 1.01±0.05 is statistically not different from one, and considering the standard error of the fitting, 0.08 μg/m^3, the intercept of the model (0.033±0.016 μg/m^3) is statistically not different from zero.

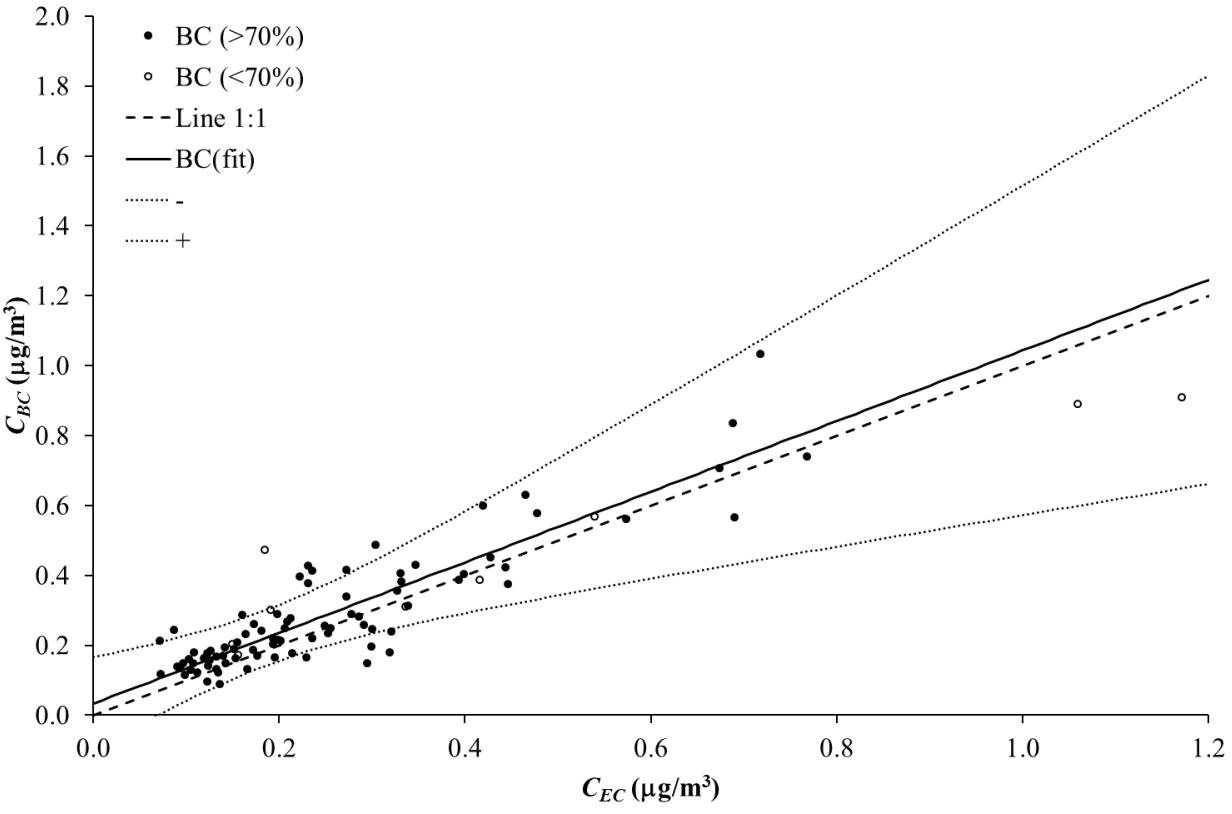

Figure 4 – Correlation plot for the concentration of black carbon (C_{BC}) and elemental carbon (C_{EC}). Black dots represent C_{BC} and C_{EC} concentrations associated with sampling periods that overlap more than 70%. Empty circles represent C_{BC} and C_{EC} concentrations associated to sampling periods that overlap less than 70%. The solid black line is the correlation model given by Eq.(5). The black dotted lines, identified as (–) and (+), are, respectively, the lower and upper limits of one standard deviation predicting interval. The dashed black line represents the 1:1 relation;

Analysis of Figure 3-b) shows that, C_{Fe}, estimated from the LV samples and from the Aethalometer show a similar behaviour, although the concentrations reported by the LV samples are systematically higher. A linear regression was performed to quantify this correlation (Figure 5) and only the pairs of points for which the Aethalometer information overlapped the LV samples by at least 70% (104 - black dots) were used for this purpose. Eq.(6) shows the model that results from this correlation analysis, with a standard error of 0.5 μg/m^3 and a correlation coefficient, *r*, of 0.96.

$$C_{Fe}\left(\mu g / m^3\right) = \left(-0.29 \pm 0.06\right) + \left(0.495 \pm 0.014\right) \times C_{Fe}\left(\mathrm{PC}; \mu g / m^3\right) \quad (6)$$

The slope of 0.495±0.014 suggests that the application of the two-component model underestimates the results given by the low volume aerosol sampler for the elemental iron by a factor of about 2. Considering the standard error of the fitting, 0.5 μg/m^3, the intercept (–0.29±0.06 μg/m^3) of the model is statistically not different from zero.

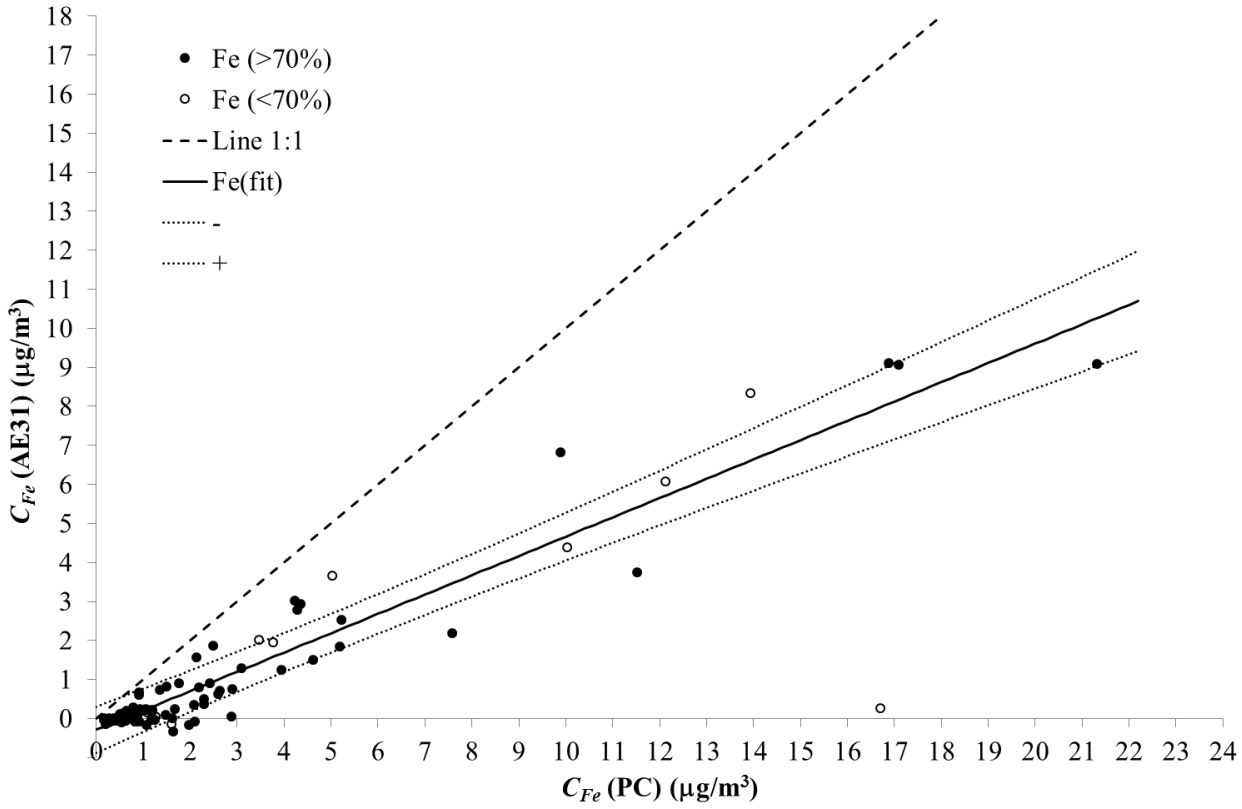

277

278 **Figure 5 –** Correlation plot for the concentration of elemental iron, C_{Fe}(AE31) calculated with the
279 Aethalometer and elemental iron, C_{Fe}(PC) calculated from the analysis of the LV
280 samples. Black dots correspond to C_{Fe}(AE31) and C_{Fe}(PC) concentrations associated
281 with sampling periods that overlap more than 70%. Empty circles represent C_{Fe}(AE31)
282 and C_{Fe}(PC) concentrations associated to sampling periods that overlap less than 70%.
283 The solid black line is the correlation model given by Eq.(6). The black dotted lines,
284 identified as (–) and (+), are, respectively, lower and upper limits of one standard
285 deviation predicting interval. The dashed black line represents the 1:1 relation.

286 The good correlation presented for the two-component model estimation of the black carbon
287 concentration (r = 0.90) and the elemental iron concentration (r = 0.96) indicates that the two-
288 component model, proposed in Eq.(1), is a good approximation for the binary interaction of these
289 two types of aerosol, since it is able to uncouple and describe the behaviour of the two optically
290 absorbing components present in the sampled aerosol.

291 Black carbon (or elemental carbon) particles are known to be associated with the aerosol fine
292 fraction (e.g. Hitzenberger and Tono, 2001; Soto-García et al., 2011). On the other hand, the
293 Aethalometer was found to be an efficient sampler for particles with an aerodynamic diameter
294 smaller than 2.5 μm (Table 1). Therefore, the instruments were appropriate to measure the total
295 concentrations of black carbon and elemental carbon, respectively, in ambient air. The slope of one

(1.01±0.05) given by (Eq.(5)) suggests that both the Aethalometer and the high volume sampler provide similar results and that the two-component model is able to estimate the black carbon concentration in a mixed aerosol containing iron dust.

Two iron classes are usually distinguished in African dust: "structural iron", mainly in the form of alumino-silicate minerals, and "free iron", in the form of oxide (hematite, Fe_2O_3) or hydroxide (goethite, FeO(OH)) discrete particles (Lafon et al., 2004). Both iron oxides and hydroxides are commonly referred to as "iron oxides" and absorb significantly in the UV-visible region (Bohren and Huffman, 1998; Linke et al., 2006). Studies performed near the northern African dust sources as well as in the Canary Islands have shown that iron oxides are more abundant in the aerosol fine fraction (Chou et al., 2008; Kandler et al., 2007). This means that during the CV-Dust field work the Aethalometer and the low volume sampler might have been collecting samples with a different proportion of iron oxides. Since the Aethalometer is sensitive to the presence of iron oxides and the iron measurements performed on the low-volume polycarbonate filters quantified total iron, it is not surprising to find a slope less than one (0.495±0.014) for Eq.6. In addition, as stated before, the low-volume sampling system was configured to collect aerosol particles with an aerodynamic diameter smaller than 10 μm and the Aethalometer was operated under efficient conditions for particles with an aerodynamic diameter smaller than 2.5 μm (Table 1). This suggests that the air reaching the filter of the Aethalometer had a lower iron concentration than the air reaching the filter of the low-volume sampler.

3.2 Influence of the loading effect on the model performance

The influence of loading effects on the performance of the two component model was evaluated with the algorithm proposed by Weingartner et al. (2003),

$$\sigma_{ATN-correct}(\lambda,t)=\frac{\sigma_{ATN-aerosol}(\lambda,t)}{R_W\left(ATN(\lambda,t),f(\lambda)\right)} \tag{7}$$

where,

$$R_W\left(ATN(\lambda,t),f\right)=\left(\frac{1}{f(\lambda)}-1\right)\times\frac{\ln\left(ATN(\lambda,t)\right)-\ln(10\,\%)}{\ln(50\,\%)-\ln(10\,\%)}+1 \tag{8}$$

The application of the above algorithm requires information about the aerosol scattering properties for the sampling site. Given that these measurements were not available for the Cape Verde atmosphere, a value of 1.203±0.031 was estimated for, by averaging, the $f(\lambda)$ values reported by Weingartner et al. (2003), for an aged external mixture of diesel soot and ammonium sulphate

particles (considering the small wavelength dependence reported, $f(\lambda)$ was assumed constant and is denoted by f).

The application of the two-component model to $\sigma_{ATN\text{-}correct}$ resulted in correlation plots similar to the ones shown in figures 4 and 5, with a small enhancement on the higher concentrations, 4% for BC (1.03 to 1.07 μg/m^3) and 13% for iron (9.1 to 10.3 μg/m^3). The new BC correlation is given by Eq.(9) and both parameters, intercept and slope, do not show any statistical difference from those given by Eq.(5),

$$C_{BC}\left(\mu g / m^3\right) = \left(0.025 \pm 0.017\right) + \left(1.02 \pm 0.06\right) \times C_{EC}\left(\mu g / m^3\right) \quad (9)$$

with a correlation coefficient, r, of 0.89 and a standard error of 0.08 μg/m^3, for the iron, the new correlation, given in Eq.(10), show a slight increase in the slope parameter by comparing with the one given by Eq.(6),

$$C_{Fe}\left(\mu g / m^3\right) = \left(-0.21 \pm 0.06\right) + \left(0.562 \pm 0.015\right) \times C_{Fe}\left(\mathrm{PC}; \mu g / m^3\right) \quad (10)$$

with a similar correlation coefficient, r = 0.96, and a standard error of 0.5 μg/m^3.

These results show that the use of a loading effect correction enhances the estimation of concentrations, and that the impact of this correction is more significant for the iron present in dust than for the BC. Although the f value used for the model was not the most appropriate for the type of aerosol sampled in Cape Verde, it is clear that the filter loading was not responsible for the 2 factor difference in the estimation of the iron concentration.

4. Conclusions

The simple two-component model, presented by Fialho *et al.* (2006), was used to remove the interference of dust (iron mineral dust) in the calculation of the BC concentrations measured with the Aethalometer. The linear regression equation that describes the relationship between BC concentrations, obtained after removing that interference, from the Aethalometer measurements and the EC concentrations that resulted from the analysis of quartz fibre filters with the thermal optical method has a slope of 1.01±0.05 and a correlation coefficient (r) of 0.90, suggesting that the two-component model provides reliable BC concentrations without interferences from iron dust.

The application of the two-component model allowed the calculation of the elemental iron concentrations in the fine particles (< 5 μm) of aerosol dust. A comparison of these concentrations with the elemental iron concentrations obtained after analysing the low-volume polycarbonate filters with the k_0-INAA technique shows a linear correlation with a slope of 0.495±0.014, an intercept of –0.29±0.06 μg/m^3 and a correlation coefficient (r) of 0.96. These results show that the

application of the two-component model to the Aethalometer data underestimated the iron concentrations in dust aerosol, which was most likely a consequence of differences in the size range of particles sampled with the Aethalometer (fine fraction) and the low-volume sampler (<10 μm) used for data comparison together with differences in the size distribution of iron oxides, which is mostly concentrated in fine particles. The high correlation obtained suggests that the assumption made before, that the enhancement of the aerosol attenuation coefficient with the wavelength was related with the iron presence in dust, is valid. If the presence of "brown" carbon was significant, this correlation coefficient would be much lower or even not significant

Finally, this study shows that the two-component model can be used as a valuable tool to remove the enhancement of the attenuation coefficient due to the presence of iron oxides in aerosol particles, and, if the presence of "brown" carbon can be neglected, at the same time, allow the estimation of the elemental iron concentration in the fine dust particles (< 5 μm).

Acknowledgements

This study was financially supported by the Portuguese Science Foundation through the project CV-Dust - Atmospheric aerosol in Cape Verde region: seasonal evaluation of composition, sources and transport (PTDD/AAC-CLI/100331/2008). The authors gratefully acknowledge the NOAA Air Resources Laboratory (ARL) for the provision of the HYSPLIT transport and dispersion model and/or READY website (http://www.ready.noaa.gov) used in this publication. Two anonymous reviewers are also acknowledged for their constructive comments and suggestions.

References

Allen, G.A., Lawrence, J., Koutrakis, P. (1999) Field validation of a semi-continuous method for aerosol black carbon (aethalometer) and temporal patterns of summertime hourly black carbon measurements in southwestern PA. Atmospheric Environment, 33, 817-823.

Almeida, S.M., Freitas, M.C., Pio, C.A, (2008). Neutron Activation Analysis for Identification of African Mineral Dust Transport, Journal of Radioanalytical and Nuclear Chemistry, 276, 161-165, http://dx.doi.org/10.1007/s10967-007-0426-4.

Almeida, S.M., Freitas, M.C., Pio, C.A., Pinheiro, M.T., Felix, P., (2013). Fifteen years of nuclear techniques application to suspended particulate matter studies. Journal of Radioanalytical and Nuclear Chemistry, 297, 347-356, http://dx.doi.org/10.1007/s10967-012-2354-1.

386 Almeida-Silva, M., Almeida, S.M., Cardoso, J., Nunes, T., Reis, M.A., Chaves, P.C., Pio, C.A.,
387 (2014) Characterization of the aeolian aerosol from Cape Verde by k0-INAA and PIXE, Journal
388 of Radioanalytical and Nuclear Chemistry, 300, 629-635,
389 http://dx.doi.org/10.1007/s10967-014-2957-9.
390 Andreae, M.O., Gelencsér, A. (2006) Black carbon or brown carbon? The nature of light-absorbing
391 carbonaceous aerosols. Atmospheric Chemistry and Physics, 6, 3131-3148.
392 Baron, P.A. (2001). Aerosol Calculator Program.
393 (http://www.tsi.com/uploadedFiles/Product_Information/Literature/Software/Aerocalc2001.xls)
394 Bodhaine, B. A. (1995). Aerosol absorption measurements at Barrow, Mauna Loa and the South
395 Pole. Journal of Geophysical Research, 100(D5), 8967 – 8975.
396 Bohren C.F., Huffman D.R. (1998). Absorption and scattering of light by small particles. Wiley
397 Interscience, Paperback Edition, New York, pg. 436-439.
398 Bond, T.C., Bergstrom, R.W. (2006) Light absorption by carbonaceous particles: an investigative
399 review. Aerosol Science and Technology, 40, 27-67,
400 http://dx.doi.org/10.1080/02786820500421521.
401 Castro, L.M., Pio, C.A., Harrison, R.M., Smith, D.J.T., (1999). Carbonaceous aerosol in urban and
402 rural European atmospheres: estimation of secondary organic carbon concentrations.
403 Atmospheric Environment 33, 2771-2781, http://dx.doi.org/10.1016/S1352-2310(98)00331-8.
404 Chou, C., Formenti, P., Maille, M., Ausset, P., Helas, G., Harrison, M., Osborne, S. (2008) Size
405 distribution, shape, and composition of mineral dust aerosols collected during the African
406 Monsoon Multidisciplinary Analysis Special Observation Period 0: Dust and Biomass-Burning
407 Experiment field campaign in Niger, January 2006 (2008) Journal of Geophysical Research, 113
408 D00C10, http://dx.doi.org/10.1029/2008JD009897.
409 Coen, M.C., Weingartner, E., Schaub, D., Hueglin, C., Corrigan, C., Schwikowski, M. and
410 Baltensperger, U. (2003). Saharan dust events at the Jungfraujoch: detection by wavelength
411 dependence of the single scattering albedo and analysis of the events during the years 2001 and
412 2002. Atmospheric Chemistry and Physical Discussion, 3, 5547 –5594.
413 Crutzen, P.J., Andreae, M.O. (1990) Biomass burning in the tropics: impact on atmospheric
414 chemistry and biogeochemical cycles. Science, 250, 1669-1678,
415 http://dx.doi.org/10.1126/science.250.4988.1669.
416 DeMott, P.J., Sassen, K., Poellot, M.R., Baumgardner, D., Rogers, D.C., Brooks, S.D., Prenni, A.J.,
417 Kreidenweis, S.M. (2003) African dust aerosols as atmospheric ice nuclei, Geophysical Research
418 Letters, 30 (14), 1732, http://dx.doi.org/10.1029/2003GL017410.

Draxler, R.R. and Rolph, G.D., (2013) HYSPLIT (HYbrid Single-Particle Lagrangian Integrated Trajectory) Model access via NOAA ARL READY Website (http://www.arl.noaa.gov/HYSPLIT.php). NOAA Air Resources Laboratory, College Park, MD.

Fialho, P., Hansen, A.D.A., Honrath, R.E. (2005) Absorption coefficients by aerosols in remote areas: a new approach to decouple dust and black carbon absorption coefficients using seven-wavelength Aethalometer data. Journal of Aerosol Science, 36, 267-282, http://dx.doi.org/10.1016/j.jaerosci.2004.09.004.

Fialho, P., Freitas, M.C., Barata, F., Vieira, B., Hansen, A.D.A., Honrath, R.E., (2006). The Aethalometer calibration and determination of iron concentration in dust aerosols. Journal of Aerosol Science, 37, 1497-1506, http://dx.doi.org/10.1016/j.jaerosci.2006.03.002.

Gonçalves, C., Alves, C., Nunes, T., Rocha, S., Cardoso, J., Cerqueira, M., Pio, C., Hillamo, R., Teinilä, K. (2014) Organic characterisation of PM_{10} in Cape Verde under Saharan dust influxes. Atmospheric Environment, 89, 425-432, http://dx.doi.org/10.1016/j.atmosenv.2014.02.025.

Hansen, A.D.A., Kapustin, V.N., Kopeikin, V.M., Gillette, D.A., Bodhaine, B.A. (1993). Optical absorption by aerosol black carbon and dust in a desert region of central Asia. Atmospheric Environment, 27A (16), 2527 – 2531.

Hansen, A. D. A. (2003). The Aethalometer Manual. Berkeley, CA, USA: Magee Scientific.

Haywood, J.; Boucher, O. (2000) Estimates of the direct and indirect radiative forcing due to tropospheric aerosols: a review. Reviews of Geophysics, 38, 513-543. http://dx.doi.org/10.1029/1999RG000078.

Hitzenberger, R., Tohno, S. (2001) Comparison of black carbon (BC) aerosols in two urban areas – concentrations and size distributions. Atmospheric Environment, 35, 2153-2167.

Jennings, S.G., Spain, T.G., Doddridge, B.G., Maring, H., Kelly, B.P., Hansen, A.D.A. (1996). Concurrent measurements of black carbon aerosol and carbon monoxide at Mace Head. Journal of Geophysical Research, 101(D14), 19447 – 19454.

Journet, E., Balkanski, Y., Harrison, S.P., (2013). A new data set of soil mineralogy for dust-cycle modeling, Atmospheric Chemistry and Physics Discussions, 13, 23943-23993, http://dx.doi.org/10.5194/acpd-13-23943-2013.

Kandler, K., Benker, N., Bundke U., Cuevas, E., Ebert, M., Knippertz, P., Rodríguez S., Schütz, L. and Weinbruch, S., (2007). Chemical composition and complex refractive index of Saharan Mineral Dust at Izaña, Tenerife (Spain) derived by electron microscopy. Atmospheric Environment, 41, 8058-8074, http://dx.doi.org/10.1016/j.atmosenv.2007.06.047.

Lafon, S., Rajot, J.-L., Alfaro, S.C., Gaudichet, A. (2004) Quantification of iron oxides in desert aerosol. Atmospheric Environment, 38, 1211-1218, http://dx.doi.org/10.1016/j.atmosenv.2003.11.006.

Langmmann, B., Duncan, B., Textor, C., Trentmann, J., van der Werf, G.R. (2009) Vegetation fire emissions and their impact on air pollution and climate. Atmospheric Environment, 43, 107-116, http://dx.doi.org/10.1016/j.atmosenv.2008.09.047.

Lieke, K., Kandler, K., Scheuvens D., Emmel, C., Von Glahn, C., Petzold, A., Weinzierl, B., Veira A., Ebert, M., Weinbruch, S., Schütz, L. (2011) Particle chemical properties in the vertical column based on aircraft observations in the vicinity of Cape Verde Islands, Tellus B, 63, 497-511, http://dx.doi.org/10.1111/j.1600-0889.2011.00553.x.

Lin, J.C., Matsui, T., Pielke Sr., R.A., Kummerow, C. (2006) Effects of biomass-burning-derived aerosols on precipitation and clouds in the Amazon Basin: a satellite-based empirical study. Journal of Geophysical Research, 111, D19204, http://dx.doi.org/10.1029/2005JD006884.

Linke, C., Möhler, O., Veres, A., Mohácsi, Á., Bozóki, Z., Szabó, G., Schnaiter M.(2006) Optical properties and mineralogical composition of different Saharan mineral dust samples: a laboratory study. Atmospheric Chemistry & Physics, 6, 3315-3323, http://dx.doi.org/10.5194/acp-6-3315-2006.

Mahowald, N.M., Baker A.R., Bergametti, G., Brooks, N., Duce, R.A., Jickells, T.D., Kubilay, N., Prospero, J.M., Tegen, I. (2005) Atmospheric global dust cycle and iron inputs to the ocean. Global Biogeochemical Cycles, 19, GB4025, http://dx.doi.org/10.1029/2004GB002402.

Park, S.S., Kim, Y.J., Fung, K. (2002) PM2.5 carbon measurements in two urban areas: Seoul and Kwangju, Korea. Atmospheric Environment, 36, 1287-1297.

Petters, M.D., Parsons, M.T., Prenni, A.J., DeMott, P.J., Kreidenweis, S.M., Carrico, C.M., Sullivan, A.P., McMeeking, G.R., Levin, E., Wold, C.E., Collet Jr., J.L., Moosmüller, H. (2009) Ice nuclei emissions from biomass burning. Journal of Geophysical Research, 114, D07209, http://dx.doi.org/10.1029/2008JD011532.

Pinnick, R.G., Fernandez, G., Andazola, E.M., Hinds, B.D., Hansen, A.D.A. and Fuller, K. (1993). Aerosol in the arid southwestern United States: measurements of mass loading, volatility, size distribution, absorption characteristics, black carbon content, and vertical structure to 7 km above see level. Journal of Geophysical Research, 98(D2), 2651 – 2666.

Pio, C.A., Cardoso, J.G., Cerqueira, M.A., Calvo, A., Nunes, T.V., Alves C.A., Custódio, D., Almeida, S.M., Almeida-Silva, M. (2014) Seasonal variability of aerosol concentration and size distribution in Cape Verde using a continuous aerosol optical spectrometer. Frontiers in Environmental Science, 2:15. http://dx.doi.org/10.3389/fenvs.2014.00015

Pio, C., Cerqueira, M., Harrison, R.M., Nunes, T., Mirante, F., Alves, C., Oliveira, C., Sanchez de la Campa, A., Artíñano, B., Matos, M. (2011). OC/EC ratio observations in Europe: Re-thinking the approach for apportionment between primary and secondary organic carbon. Atmospheric Environment 45, 6121-6132, http://dx.doi.org/10.1016/j.atmosenv.2011.08.045.

Prospero, J.M., Ginoux, P., Torres, O., Nicholson S.E., Gill, T.E. (2002) Environmental characterization of global sources of atmospheric soil dust identified with the Nimbus 7 total ozone mapping spectrometer (TOMS) absorbing aerosol product, Review of Geophysics, 40(1), 1002, http://dx.doi.org/10.1029/2000RG000095.

Rolph, G.D., (2013) Real-time Environmental Applications and Display sYstem (READY) Website (http://www.ready.noaa.gov). NOAA Air Resources Laboratory, College Park, MD.

Satheesh, S.K., Krishna Moorthy, K. (2005) Radiative effects of natural aerosols: a review. Atmospheric Environment, 39, 2089-2110, http://dx.doi.org/10.1016/j.atmosenv.2004.12.029.

Schmid, H., Laskus, L., Abraham, H. J., Baltensperger, U., Lavanchy, V., Bizjak, M., Burba, P., Cachier, H., Crow, D., Chow, J., Gnauk, T., Even, A., ten Brink, H. M., Giesen, K., Hitzenberger, R., Hueglin, C., Maenhaut, W., Pio, C., Carvalho, A., Putaud, J.-P., Toom-Sauntry, D. & Puxbaum, H. (2001). Results of the "carbon conference" international aerosol carbon round robin test stage I, Atmospheric Environment, 35, 2111-2121.

Soto-García, L.L., Andreae, M.O., Andreae, T.W., Artaxo, P., Maenhaut, W., Kirchstetter, T., Novakov, T., Chow, J.C., Mayol-Bracero, O.L. (2011) Evaluation of the carbon content of aerosols from the burning of biomass in the Brazilian Amazon using thermal, optical and thermal-optical analysis methods. Atmospheric Chemistry and Physics, 11, 4425-4444.

Tesche, M., Gross, S., Ansmann, A., Müller D., Althausen, D., Freudenthaler, V., Esselborn, M. (2011) Profiling of Saharan dust and biomass-burning smoke with multiwavelength polarization Raman lidar at Cape Verde, Tellus B, 63, 649-676, http://dx.doi.org/10.1111/j.1600-0889.2011.00548.x.

Torrent, J., Schwertmann, U., Fechter, H., Alferez, F. (1983) Quantitative relationships between soil color and hematite content, Soil Science, 136(6), 354-358.

Weingartner, E., Saathoff, H., Schnaiter, M., Streit, N., Bitnar, B., Baltensperger, U. (2003) Absorption of light by soot particles: determination of the absorption coefficient by means of aethalometers, Journal of Aerosol Science, 34, 1445-1463.